High-performance nanogap electrode-based impedimetric sensor for direct DNA assays

Hyunjung Lee, Joo Oak Keem, Hyunmin Cho, Jong Min Choi, Won Seok Chung, Dae-Young Jeon, Dong Su Lee, Yong-Beom Shin

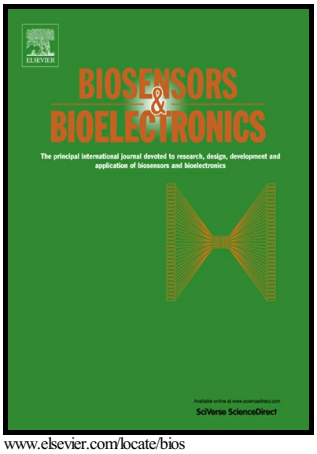

www.elsevier.com/locate/bios

PII: S0956-5663(18)30550-5
DOI: https://doi.org/10.1016/j.bios.2018.07.050
Reference: BIOS10639

To appear in: *Biosensors and Bioelectronic*

Received date: 16 May 2018
Revised date: 23 July 2018
Accepted date: 25 July 2018

Cite this article as: Hyunjung Lee, Joo Oak Keem, Hyunmin Cho, Jong Min Choi, Won Seok Chung, Dae-Young Jeon, Dong Su Lee and Yong-Beom Shin, High-performance nanogap electrode-based impedimetric sensor for direct DNA assays, *Biosensors and Bioelectronic,* https://doi.org/10.1016/j.bios.2018.07.050

High-performance nanogap electrode-based impedimetric sensor for direct DNA assays

Hyunjung Lee[a*], Joo Oak Keem[a], Hyunmin Cho[a], Jong Min Choi[a], Won Seok Chung[a], Dae-Young Jeon[b], Dong Su Lee[b], Yong-Beom Shin[a,c*]

[a]*BioNano Health Guard Research Center (H-GUARD), Daejeon 34141, Republic of Korea*

[b]*Institute of Advanced Composite Materials, Korea Institute of Science and Technology, Jeonbuk 55324, Republic of Korea*

[c]*Hazards Monitoring Bionano Research Center, Korea Research Institute of Bioscience and Biotechnology (KRIBB), Daejeon 34141, Republic of Korea*

hjunglee@kribb.re.kr

ybshin@kribb.re.kr

Abstract

The rapid and sensitive detection of pathogen DNA (Deoxyribonucleic acid) would be essential for diagnosis and appropriate antibiotic treatment time. Herein, we report a novel

direct DNA detectable impedimetric sensor. Direct assay of the amplified target DNA (*mecA* gene from methicillin-resistant *Staphylococcus aureus* (MRSA)) was performed using the PCR (polymerase chain reaction) product without any purification. Even though there are lots of PCR reagents and excess salts in sample PCR product, the nanogap electrode-based impedimetric sensor was able to detect DNA amplification fast in 5^{th} PCR cycle which had 260 fM *mecA* gene in sample originally. The 70 nm gap electrode sensor yielded over 20 % signal increase at the 5^{th} PCR cycle and the impedance change grew up to about 60 % at 25^{th} in case of sample with 260 fM *mecA* gene template originally. The increased concentration of target DNA template led to the rise in impedance change such as 60 % up at 5^{th} and 120 % up at 25^{th} cycle with 260 pM, respectively. It is very outstanding result as compared with the traditional PCR agarose gel. Besides, it is 7-fold superior sensitivity to the microgap electrode. Furthermore, genomic DNA sample extracted from MRSA was detected rapidly. The nanogap electrode-based impedimetric sensor could be a good candidate for a rapid, sensitive, and low-cost electrical biosensor for DNA characterization in diagnostics and disease monitoring.

Keywords: Nanogap; Impedimetric sensor; Direct DNA assay; *MecA* gene; Theoretical calculation; Label-free

1. Introduction

The detection of pathogen has been an important issue for preventing nosocomial disease. Analysis time and sensitivity are critical limitations related to the performance of microbiological test. The effective testing of pathogen is required many complex methods to ensure bacteria, so the detecting results are not available in time. Therefore lots of detection instruments have been developed using various techniques of detection such as immunomagnetic separations, flow cytometry, polymerase chain reaction (PCR), loop-mediated isothermal amplification (LAMP), bioluminescence (Hibi et al., 2006; Yang et al., 2006; Kempf et al., 2005; Jonas et al., 2002; Greisen et al., 1994; Wang et al., 2015; Prosser et al., 1996). However, many of these methods are still time-consuming.

Electrical and electrochemical analyses have been reported as some of the most promising, simple, and sensitive detection techniques with rapid responses in biological sample assays. (Abdel-Hamid et al., 1999; Brewster et al., 1998; Gehring et al., 1998; Su et al., 2004; Drummond et al., 2003; Park et al., 2002). In particular, an electrical impedance biosensor could be a fast, cost-effective, and readily compatible technique that can be used in modern electronic facilities. Most impedimetric sensors measure the impedance change over a wide frequency range from an affinity-based surface reaction on an electrode, such as DNA hybridization, an immunoreaction, and sometimes a signal amplification reaction by an enzymatic or electrochemical method (Drummond et al., 2003; Sharma et al., 2016; Radhakrishnan et al., 2014; Wang et al., 2012; Luo et al., 2011; Timms et al., 1996; Katz et al., 2003; Guan et al., 2004; Andrzej, 2014; Hammond et al., 2016). These reactions require the expensive labelling step of capturing probe molecules on the electrode surface, the affinity binding step between capturing probe and target, and the several washing steps to remove unbinding molecules. Those make the measurement process complex. Moreover, the

electrode chip combined with the target molecules are only single-use. Various nanomaterial-based electrochemical biosensors which do not needed the direct functionalization of electrode have been studied, but, it is necessary to pre-treatment process and time for functionalization on those materials (Palchetti et al., 2012; Csordas et al., 2010; Kurlyandskaya et al., 2007; Wang et al., 2013; Ghindilis et al., 2009).

In contrast, the direct sample analysis of the bulk solution impedance would overcome the limitation for about the complex pre-treatment of affinity-based sensors. Many studies on a label-free impedance sensor for the DNA characterization after PCR have been reported; however, those methods prepare the target DNA sample by purification such as gel extraction after PCR, ethanol precipitation and resuspension in deionized water for the measurements (Ma et al., 2013; Liu et al., 2008; Salm et al., 2011). It is due to that lots of salt ions and single-strand DNAs such as primer, probe, dNTP (deoxynucleoside triphosphate) in PCR solution would accumulate on the electrode surface and form an electric double layer, which caused electrode polarization. Electrode polarization is a major factor of error in measuring the impedance of biomolecules in high-salt solutions (Liu et al., 2008; Schwan, 1996).

To minimize the effect of electrode polarization, we designed a nanogap electrode-based impedimetric sensor and directly analyzed the electrical bulk solution impedance of high-salt PCR sample solution without any DNA purification. The PCR solutions were prepared after different numbers of PCR cycles. Due to controlled PCR cycles, the target DNA *(mecA* gene) which is defining standard of MRSA was differently amplified depending on the cycles. MRSA is one of high concerned pathogen in health medical fields because of its diverse array of fatal infections (Pournajaf et al., 2014; Ghanwate et al., 2016; Stürenburg et al., 2009; Robicsek et al., 2008; Struelens et al., 2009; Hulme, 2017), and the fast identification of

MRSA would be of tremendous clinical benefit because it would allow administration of the appropriate antibiotic treatment. Therefore, we measured the bulk solution impedance of PCR products at different stages of amplification of the target *mecA* gene according to the PCR cycle by a nanogap electrode-based impedimetric sensor for rapid detection.

2. Materials and methods

2.1. Preparation of PCR product samples

Plasmid DNA containing the *mecA* gene was used as the DNA template for PCR. The sequences for amplification were derived from an already well-known region of the *mecA* gene. All oligonucleotides were synthesized by Macrogen (South Korea). A forward primer sequence (GGCAATATTAACGCACCTCA) and reverse primer sequence (GTCTGCCAGTTTCTCCTTGT) were used for amplification of a 200 bp region. For each reaction, we added 0.2 μM dNTPs and 0.4 μM forward and reverse primers. PCR was carried out using a TAKARA PCR thermocycler. The protocol for PCR was as follows: 95 ℃ for 5 min (initial denaturation), 95 ℃ for 30 sec (denaturation), 55 ℃ for 30 sec (annealing), and 72 ℃ for 25 sec (extension). PCR sample products with different amounts of the amplified *mecA* gene were prepared by controlling the number of cycles. During PCR, nonspecific DNA amplification occurred with many PCR cycles (over 35) even though there was no target template in the PCR mixture. Therefore, we carried out PCR at up to 25 cycles to prevent nonspecific amplification in the assay samples. Each 10 μl of PCR products injected on the nanogap electrode chip sensor was electrophoresed on agarose gel to confirm the amplified target DNA band. The relative intensity of target DNA band which is designated

area by yellow box in gel photo was measured numerically using Image J (Image processing and analysis in Java) program by following equation;

$$\text{Relative intensity} = \frac{I_{i\ cycle} - I_{0\ cycle}}{I_{0\ cycle}}$$

where $I_{0\ cycle}$ is an intensity of 0^{th} PCR cycle (no PCR process), $I_{i\ cycle}$ is an intensity of i^{th} cycle of each photo, respectively.

The methicillin-resistant *Staphylococcus aureus* (MRSA; ATCC 43300) and *Staphylococcus aureus* (SA; KCTC 1621) was purchased from the American Type Culture Collection (ATCC, USA) and Korean Collection for Type Cultures (KCTC, South korea), respectively. The MRSA and SA cells were cultured in LB broth (BD, USA) for overnight at 37 ℃. Cells were harvested, and MRSA and SA genomic DNA (gDNA) extracted using G-Spin Total DNA Extraction Kit (iNtRON, South Korea) according to the manufacture's protocol. The isolated genomic DNA was quantified using the NanoDrop 2000c Spectrophotometer (Thermo Scientific, USA) and used as DNA template for real sample.

2.2. Fabrication of the nanogap electrode chip and impedimetric sensor

The nanogap electrode chips were fabricated on 8 inches of a silicon oxide wafer by two rounds of insulator deposition and photolithography. First, the deposition of silicon oxide (SiO_2) and silicon nitride (Si_3N_4) using low-pressure chemical vapor deposition (LPCVD) and etching created an approximately 500 nm gap structure on the wafer. The narrower nanogap structure was created by secondary silicon nitride deposition. Finally, titanium/gold layers were deposited perpendicularly onto the nanostructure. As a result, more than 1,000 ea. nanogap electrode chips could be made through only one process. Before use, the nanogap

electrode chips were cleaned with acetone, ethanol, and deionized water, and then were dried with a nitrogen. In addition, a gold IDA (interdigitated array) electrode with a 2 μm width and 2 μm gap was purchased from ALS Co., Ltd. (Japan). A PDMS (polydimethylsiloxane) well with a 2 mm hole was fixed on the electrodes after O_2 plasma treatment and was adhered by epoxy to designate the same working area on each electrode. The impedimetric sensor was fabricated by mounting the electrode chips on sensor zig and connecting them to an external impedance apparatus.

2.3. Electrical impedance characterization and electric field simulation

A ZIVE BP2C (WonATech, South Korea) electrochemical workstation was used to apply bias at 50 mV DC and a sine-modulated AC potential with a 10 mV_{pp} amplitude for measurement over the frequency range from 1 Hz to 1 MHz. PCR product (5 μl) was injected into the PDMS well on the electrode chip of the impedance sensor, and then the well was covered by a flat PDMS lid. Finally, the sensor was enclosed by an aluminum foil box to minimize external noise during measurement of the bulk solution electrical impedance.

FlexPDE software based on scripted finite element models was used for numerical simulation of the E-field distribution in the vicinity of the fabricated electrodes. First, 50 nm thick electrodes and a 300 nm thick SiO_2 layer were defined. In addition, the relative dielectric constant of the electrolyte was assumed to be 80 and 1, respectively. The bias of 10 mV_{pp} was applied to the electrodes.

3. Results and discussion

3.1. Electrical impedance measurement of sodium chloride aqueous solution and the equivalent circuit of the nanogap-based impedimetric sensor

A schematic diagram about the fabrication of nanogap electrode and a configuration of sensor chip were shown in Fig. S1. A SEM (Scanning electron microscope) image (Fig. S1b) was shown gold (Au) electrode and titanium (Ti) adhesive layer were deposited on silicon nitride (Si_3N_4) nanogap structure. With a yield of over 90 %, approximately 1,000 ea. electrode chips with nanogap gap could be fabricated in one process. In addition, the nanogap electrode retained a resistance of over 10^{13} ohms on average. At first, the stability of the impedance signal was investigated by repeatedly measuring the impedance of deionized water (DW) and a PCR mixture without the target *mecA* gene template using the same 70 nm nanogap electrode chip at 125 Hz. As a result, uniform bulk solution impedances with standard deviations below 1.4 % and 0.6 % were obtained over five replicate measurements in both cases (shown in Fig. S2). Therefore, there is almost no impedance change when measuring the same sample by our assay using the nanogap electrode-based impedimetric sensor, and the background noise of this sensor is 2 % or less. To verify the measurement performance of our nanogap electrode-based impedimetric sensor, the bulk solution impedance of aqueous sodium chloride (NaCl) solutions of different concentrations was analyzed using a sensor that had various gap distances between opposing electrodes: a 70, 150, 300, and 500 nm nanogap and a 2 μm microgap. As confirmed in Fig. S3a and S3b, the 70 nm nanogap electrode-based sensor more distinctly detected slight differences in bulk solution electrical impedance according to the concentration of the NaCl solution than the 2 μm microgap electrode-based sensor. For the 70 nm nanogap sensor, a plateau in the Bode plot of $Z_{Magnitude}$-Frequency (Z_{Mag}-F), which is due to the resistance of the solution (R_s), can

be observed over a wide salt concentration from 85.6 mM to 53 nM (Fig. S3a). In contrast, the bulk solution impedance increased only at 5.3 mM NaCl solution with the 2 μm microgap electrode sensor. Solutions with a salt concentration less than 5.3 mM showed almost same impedance as pure water, and only subtle changes appeared at higher salt concentrations (Fig. S3b). As shown in Fig. S3c, we graphed the impedance data and their linear fitting for both the 70 nm nanogap and 2 μm microgap sensors on one plot. The impedance data from the 2 μm microgap electrode sensor obtained at 2.5 kHz showed most spread. With the 70 nm nanogap electrode sensor, the frequency corresponding to each data point was different, for example, 126, 63, 32, 20, and 8 kHz and 631, 100, 40, 25, and 20 Hz, from 85.6 mM to 53 nM, respectively. The data from both impedimetric sensors showed linear correlations, but the data from the nanogap electrode-based sensor presented sharper changes. Changes in the normalized impedance with different concentrations of NaCl according to the gap size are summarized in Fig. 1. As the NaCl concentration increases in solution, many more active ions exist, and the solution resistance is the main effective factor determining the impedance. Therefore, the Z_{Mag} bode plot shifts to a high-frequency regime (shown in Fig. S3a), which means a highly conductive solution, and this stiff changes were particularly noticeable with smaller gap electrode sensors (Fig. 1). The impedance of the nanogap electrode-based sensors drastically decreased by approximately 88 % and 91 % with the salt concentration for gaps of 150 nm and 70 nm, respectively. While the impedance change with the microgap electrode declined gradually and ultimately decreased by 38 %. Considering that repeated measurements with the 70 nm nanogap electrode sensor resulted in an impedance variation of less than 2 %, as shown in Fig. S2, it was confirmed that these nanogap electrode-based impedimetric sensors perform well when analyzing the variation in the bulk solution

electrical impedance with the salt concentration. Typically, the impedance spectrum of an electrolyte solution can be separated into three different regimes, i.e., the double-layer region, solution-resistance region and dielectric region, depending on the dominant circuit elements in the specific frequency range. As suggested in Fig. S4a, an equivalent circuit model of the electrical behaviors consistent with the three components was constructed, including the dielectric capacitance (C_{di}) of the solution surrounding the electrodes; the resistance of the solution (R_s); and the constant phase elements (Z_{CPE}), which is the interfacial impedance of a double-layer capacitance between the electrode and solution (McAdams et al., 1995; Gerwen et al., 1998). The total impedance (Z_{Mag}) from the equivalent circuit model was calculated by equation (1):

$$Z_{Mag}{}^{-1} = \frac{1}{2 \cdot Z_{CPE} + R_s} + j\omega \cdot C_{di} \quad (1)$$

The constant phase elements could be affected by the roughness of the electrode surface (McAdams et al., 1995) and are thus expressed as below:

$$Z_{CPE} = \frac{1}{B(j\omega)^{\beta}} \quad (2)$$

where ω is the angular frequency, *B* is the inverse of the absolute value of Z_{CPE} at ω=1, and β is the fractional exponent related to the electrode topography. The Z_{CPE} of the double-layer region was dominantly expressed in the low-frequency range. The solution resistance (R_s) can be observed in the intermediate-frequency range, namely, a peak in the phase signal corresponding to the plateau in the Bode plot can be relevant in this region. The peak point in the phase appears at a relatively low frequency for a high-resistance solution and shifts to the high-frequency region for a low-resistance solution. As indicated in Fig. S3a, the nanogap

electrode-based impedimetric sensor explicitly presented three different regimes, the double-layer region, solution resistance region, and dielectric region, according to the three domain circuit elements operating in specific frequency ranges. For a more quantitative analysis, three different phase plots (0, 530 μM, and 85.6 mM NaCl) were nonlinearly fitted by Eq. (3) based on the equivalent circuit model in Fig. S4a:

$$\theta = tan^{-1}\left[\frac{Z_{Im}}{Z_{Re}}\right] = tan^{-1}\left[\frac{C_{di}\omega^{1-\beta}\left(4+B^2{R_s}^2\omega^{2\beta}\right)+4C_{di}BR_s\omega\cdot\cos\left(\frac{\beta\pi}{2}\right)+2B\cdot\sin\left(\frac{\beta\pi}{2}\right)}{B\left(BR_s\omega^{\beta}+2\cos\left(\frac{\beta\pi}{2}\right)\right)}\right]\times 180°/\pi \qquad (3)$$

where Z_{Re} and Z_{Im} denote the real and imaginary parts of the total impedance (Z_{Mag}), respectively. The value of the fractional exponent (β) related to the surface roughness of the electrode was fixed because the impedance was measured by the same electrode. More than 95 % of the experimental data were fit well by the equivalent circuit model (Fig. S4b), and the theoretically calculated values of the model parameters are summarized in Table S1. As the salt concentration increased, the solution resistance greatly decreased with a large increase in electrical conductivity, so the bulk solution impedance changed primarily according to the resistance component. Therefore, the phase shifted into the high-frequency region dramatically. In addition, the dielectric capacitance decreased because of a nonrapid alignment of charge molecules in the electrolyte, and the double layer was thinned further because of the increase in double-layer capacitance. As a result, the nanogap electrode-based impedimetric sensor shows a very reasonable trend and obvious performance. In addition, the data are linearly related to the NaCl concentration and match well with the theoretical calculations. Therefore, an assay with the nanogap electrode-based impedimetric sensor is a practical and effective apparatus for the analysis of the bulk solution impedance even in high-salt solutions.

Additionally, for verification of the effect of the exposed working area on the sensor sensitivity to the bulk solution impedance, we evaluated sodium chloride solution assays using two electrodes with the same gap size of 70 nm and different exposed working areas: 4.8×10^3 μm^2 and 2×10^5 μm^2. The electrode with a small working area (4.8×10^3 μm^2) detected no impedance changes, while the large electrode (2×10^5 μm^2) detected clear impedance changes according to the NaCl concentration (Fig. S5). Therefore, it was confirmed that in addition to a narrowed nanogap, an exposed working area of at least 1×10^5 μm^2 is necessary for the efficient measurement of impedance. Therefore, all of nanogap-based impedimetric sensors were fabricated with a working area of at least 2×10^5 μm^2.

3.2. Electrical impedance assay of PCR products

We tested a 10 μl PCR product with various concentrations of the *mecA* plasmid template from 260 pM to 260 fM; the template DNA amplification was previously confirmed by the agarose gel (Fig. S6a) and the relative intensity of target DNA bands (yellow dot line region) in agarose gel was plotted (Fig. S6b). The DNA amplification was confirmed beginning at the 8th PCR cycle in the sample with 260 pM template, but the band was observed from 15th and 20th PCR cycles in the samples with much less of the target template, 2.6 pM and 260 fM, respectively. First, 5 μl of the 260 pM template solution was placed on the designated working area of the electrode, and the bulk solution electrical impedance was measured by modulating the frequency as depicted in Fig. 2 and Fig. S7. Fig. 2a and 2b show Bode plots expressing the impedance magnitude of the frequency response, and Fig. S7a and S7b present Nyquist plots of the nano- and microgap electrode sensors, respectively. The magnitude of the bulk solution electrical impedance clearly increased as PCR proceeded, and this increase is attributed to the target DNA template amplification during PCR in the presence of the

template. In the DNA assay using the PCR product, the total concentration of ionic molecules did not change, and only the size of typical ionic molecules, namely, nucleoside triphosphates (dNTPs), became larger to form DNA by amplification. It could be reasoned that the overall ion mobility was disrupted in samples, which was reflected in the total solution impedance growth shown in Fig. 2a, and the peak of the phase shifted to the higher frequency region corresponding to that in Fig. S8. However, there were almost no impedance changes for the PCR product without template, the DNA of which was not amplified even though the same 70 nm nanogap electrode was used (Fig. S9). The Nyquist plots of the PCR products with template were spread more widely according to the number of PCR cycles (Fig. S5a vs. Fig. S9b). Different from the impedance changes with variations in the concentration of the NaCl solution, the changes in bulk solution impedance of the PCR products were relatively small. This result is related to the uniform concentration of ionic molecules in the PCR products. That is, we altered the amount of NaCl in the samples artificially, but the amount of the components in the PCR product were fixed; the only change was the size of the ionic molecules from the natural conversion of dNTP to DNA as PCR proceeded. For a more sensitive analysis, we fit the measured data to the equivalent circuit model. Approximately 97 % of the data were fitted well, and the theoretical calculations are described in Table S2. As the amount of target DNA increased with increasing PCR cycles, the solution resistance decreased because DNA is highly negative charged and could behave as a mobile charge carrier. The dielectric capacitance (C_{di}) increased due to the enhanced dipole moments of the amplified DNA backbone after PCR. In addition, the PCR product contained many ionic molecules, and the double layer became thinner; thus, the electric double-layer capacitance (B) increased. The impedance changes observed for the same PCR product using the

microgap electrode sensor are presented in Fig. 2b and S5b. Even though the same sample was analyzed as in the case of the nanogap electrode sensor (Fig. 2a and S5a), only subtle impedance changes could be measured with the microgap electrode sensor; moreover, there were not three clear regimes corresponding to the types of electric behavior.

3.3.Performance of nanogap-based impedimetric sensor

Fig. 3 presents the normalized magnitude of the bulk solution impedance at 126 Hz with different concentrations of template in each sample according to the PCR cycle. Numerically, 178 % of the impedance at 126 Hz increased from cycle 0 to cycle 20 with the 70 nm nanogap electrode sensor, while only 40 % changed at 2 kHz with the 2 μm microgap sensor. This result shows the sensitivity of nanogap electrode sensor is better than that of microgap electrode sensor for evaluation of electrical solution properties. Unlike the sample with the 260 pM template, the control group with no template presented a smaller change of approximately 22 % even though the same nanogap electrode sensor chip was used. The higher background noise of the 70 nm nanogap electrode sensor, however, verified that there was more significant impedance growth corresponding to the target DNA amplification. The normalized impedance at same frequency differed according to the template concentration at each PCR cycle using the nanogap electrode chip with a uniform 70 nm gap size (Fig. 4). The PCR product from the 260 fM template originally was clearly distinguished at the 5^{th} cycle from the background noise with the 70 nm nanogap electrode-based impedimetric sensor, which was confirmed in the gel band obtained beginning at the 20^{th} cycle of PCR. In addition, it was clearly confirmed that an electrode sensor with a much narrower gap size could yield high impedance changes corresponding to the amount of DNA amplification, as shown in Fig. 5. We simulated the electric field distribution in the electrolyte around the electrode by

FlexPDE software (Fig. S10). Regardless of the large differences about the relative dielectric constant of the solution, the electric field induced in the electrode was overlapped with one of its counter electrode in case of the 70 nm nanogap and as a result, a relatively strong electric field was sustained across the nanogap. The intensity distribution of electric field between electrodes was more uniform in the 70 nm nanogap, which leads to that the net change of ion density becomes nearly zero within the nanogap. Therefore, electrode polarization is minimized in the nanogap electrode sensor, and the potential drop and signal loss resulting from the unwanted electric double-layer effect are significantly reduced. Consequently, the electric field was built up within nanogap between the two electrodes but was not in the microgap, meaning that even small changes between the electrodes can be sensitively detected by the nanogap electrode sensor. Thus, the sensitivity of the nanogap-based impedimetric sensor is increased for the measurement of impedance changes according to subtle differences in the sample molecules. As a result, the smaller nanogap electrode sensor has high sensitivity for direct DNA characterization even in high-salt solutions. The amplification of genomic DNA (gDNA, 3*,000 kbp; McClure et al., 2017*) extracted from MRSA was assayed efficiently as shown in Fig. 6. In agarose gel of PCR product with 531 fM gDNA, it could be clearly confirmed from 20^{th} cycle (Fig. 6a). However, the nanogap sensor was able to detect an increment of gDNA obviously from 5^{th} PCR cycle as shown in Fig. 6b and it was very fast assay compared with a result of agarose gel. Therefore the nanogap electrode based-impedimetric sensor could analyzed a real gDNA from MRSA clearly and rapidly even in PCR product without any purification.

Conclusions

The nanogap electrode-based impedimetric sensor were successfully applied to direct detection of DNA amplification in PCR product by measuring subtle changes in the bulk solution impedance. There were strong correlations between the electrical impedance and DNA amplification. The nanogap electrode-based impedimetric sensor was able to detect in 5^{th} PCR cycle of sample which was contained 260 fM *mecA* DNA originally. Considering that the amplification of *mecA* gene could be confirmed from 20^{th} cycle in agarose gel analysis with same sample, the nanogap impedimetric sensor was suitable for rapid monitor of DNA amplification. In addition, 70 nm nanogap sensor achieved the maximum 7-fold superior sensitivity to microgap electrode sensor. In addition, it does not require any pre-treatment for DNA purification such as magnetic separation, centrifuge precipitation or filtration. It is considered that the nanogap reduces the electrode polarization between electrodes, which minimizes the electrical potential drop and unwanted electric double-layer effect during the assay. The electrode with much narrower gap and larger working area showed high sensitive performance. The 70 nm nanogap sensor was effectively assayed the amplification of genomic DNA which was extracted from MRSA.

The nanogap electrode-based impedimetric sensor has a potential to be used as a very sensitive, miniaturized electric devices for the direct assay of DNA and pathogen. Future research would be needed to further reduce the detection limit and apply the sensor to commercial devices.

Acknowledgements

This work was supported by the BioNano Health-Guard Research Center funded by the

Ministry of Science and ICT (MSIT) of Korea as a Global Frontier Project (Grant number H-GUARD_2013M3A6B2078950).

D. Jeon acknowledges support from the Korea Institute of Science and Technology (KIST) Institutional Program and the programs through the National Research Foundation of Korea (NRF) funded by the Ministry of Science, ICT and Future Planning (NRF-2017M3A7B4049167).

References

Hibi, K., Abe, A., Ohashi, E., Mitsubayashi, K., Ushio, H., Hayashi, T., Ren, H., Endo, H., 2006. Combination of immunomagnetic separation with flow cytometry for detection of Listeria monocytogenes. Anal. Chim. Acta 173-174, 158-163.

Yang, L., Li, Y., 2006. Detection of viable Salmonella using microelectrode-based capacitance measurement coupled with immunomagnetic separation. J. Microbiol. Methods 64, 9-16.

Kempf, V.A., Mändle, T., Schumacher, U., Schäfer, A., Autenrieth, I.B., 2005. Rapid detection and identification of pathogens in blood cultures by fluorescence in situ hybridization and flow cytometry. Int. J. Med. Microbiol. 295, 47-55.

Jonas, D., Speck, M., Daschner, F.D., Grundmann, H., 2002. Rapid PCR-Based Identification of Methicillin-Resistant Staphylococcus aureus from Screening Swabs. J. Clin. Microbiol. 40, 1821-1823.

Greisen, K., Loeffelholz, M., Purohit, A., Leong. D., 1994. PCR primers and probes for the

16S rRNA gene of most species of pathogenic bacteria, including bacteria found in cerebrospinal fluid. J. Clin. Microbiol. 32, 335-351.

Wang, X., Wu, L., Wang, Y., Ma, Y., Chen, F., Ou, H., 2015. Rapid detection of *Staphylococcus Aureus* by Loop-mediated isothermal amplification. Appl. Biochem. Biotechnol. 175, 882-891.

Prosser, J.I., Killham, K., Glover, L.A., Rattray, E.A., 1996. Luminescence-based systems for detection of bacteria in the environment. Crit. Rev. Biotechnol. 16, 157-183.

Abdel-Hamid, I., Ivnitski, D., Atanasov, P., Wilkins, E., 1999. Flow-through immunofiltration assay system for rapid detection of E. coli O157:H7. Biosens. Bioelectrons. 14, 309-316.

Brewster, J.D., Mazenko, R.S., 1998. Filtration capture and immunoelectrochemical detection for rapid assay of Escherichia coli O157:H7. J. Immunol Methods 211, 1-8.

Gehring, A.G., Patterson, D.L., Tu, S.I., 1998. Use of a Light-Addressable Potentiometric Sensor for the Detection of Escherichia coli O157:H7. Anal. Biochem. 258, 293-298.

Su, X.L., Li, Y., 2004. A self-assembled monolayer-based piezoelectric immunosensor for rapid detection of Escherichia coli O157:H7. Biosens. Bioelectrons. 19,563-574.

Drummond, T.G., Hill, M.G., Barton, J.K., 2003. Electrochemical DNA sensors. Nat. Biotechnol. 21, 1192-1199.

Park, S.J., Taton, T.A., Mirkin, C.A., 2002. Array-based electrical detection of DNA with nanoparticle probes. Science, 295, 1503-1506.

Sharma, R., Deacon, S.E., Nowak, D., George, S.E., Szymonik, M.P., Tang, A.A.S.,

Tomlinson, D.C., Davies, A.G., McPherson, M.J., Wälti C., 2016. Label-free electrochemical impedance biosensor to detect human interleukin-8 in serum with sub-pg/ml sensitivity. Biosens. Bioelectrons. 80, 607-613.

Radhakrishnan, R., Suni, I.I., Bever, C.S., Hammock, B.D., 2014. Impedance biosensors: Applications to sustainability and remaining technical challenges. ACS Sustainable Chem. Eng. 2, 1649-1655.

Wang, Y., Ye, Z., Ying, Y., 2012. New trends in impedimetric biosensors for the detection of foodborne pathogenic bacteria. Sensors 12, 3449-3471.

Luo, X., Xuan, F., Hsing, I., 2011. Real time electrochemical monitoring of PCR amplicons using electroactive hydrolysis probe. Electrochem. Commun. 13, 742-745.

Timms, S., Colquhoun, K.O., Fricker, C.R., 1996. Detection of Escherichia coli in potable water using indirect impedance technology. J. Microbiol. Methods 26, 125-132.

Katz, E., Willner, I., 2003. Probing Biomolecular Interactions at Conductive and Semiconductive Surfaces by Impedance Spectroscopy: Routes to Impedimetric Immunosensors, DNA-Sensors, and Enzyme Biosensors. Electroanalysis 15, 913-947.

Guan, J.G., Miao, Y.Q., Zhang, Q.J., 2004. Impedimetric biosensors. J. Biosci. Bioeng. 97, 219-226.

Andrzej, L., 2014. Electrochemical Impedance Spectroscopy and its Applications. Springer DOI 10.1007/978-1-4614-8933-7.

Hammond, J.L., Rosamond, M.C., Sivaraya, S., Marken, F., Estrela, P., 2016. Fabrication of a horizontal and a vertical large surface area nanogap electrochemical sensor. Sensors 16,

2128-2143.

Palchetti, I., Mascini, M., 2012. Electrochemical nanomaterial-based nucleic acid aptasensors. Anal. Bioanal. Chem. 402, 3103-3114.

Csordas, A., Gerdon, A.E., Adams, J.D., Qian, J., Oh, S.S., Xiao, Y., Soh, H.T., 2010. Detection of proteins in serum by micromagnetic aptamer PCR (MAP) technology. Angew. Chem. Int. Ed. 49, 355-358.

Kurlyandskaya, G.V., Fal, M.V., 2007. Surface modified amorphous ribbon based magnetoimpedance biosensor. Biosens. Bioelectrons. 22, 2341-2345.

Wang, T., Zhou, Y., Lei, C., Lei, J., Yang, Z., 2013. Ultrasensitive detection of Dynabeads protein A using the giant magnetoimpedance effect. Microchim. Acta 180, 1211-1216.

Ghindilis, A.L., Smith, M.W., Schwarzkopf, K.R., Zhan, C., Evans, D.R., Baptista, A.M., Simon, H.M., 2009. Sensor Array: Impedimetric label-free Sensing of DNA hybridization in real time for rapid, PCR-based detection of microorganisms. Electroanalysis 21, 1459-1468.

Ma, H., Wallbank, R.W.R., Chaji, R., Li, J., Suzuki, Y., Jiggins, C., Nathan, A., 2013. An impedance-based integrated biosensor for suspended DNA characterization. Sci. Rep. 3, 2730 (doi:10.1038/srep02730).

Liu, Y., Banada, P.P., Bhattacharya, S., Bhunia, A.K., Bashir, R., 2008. Electrical characterization of DNA molecules in solution using impedance measurements. Appl. Phys. Lett. 92, 143902-143902-3.

Salm, E., Liu, Y., Marchwiany, D., Morisette, D., He, Y. Bhunia, A.K., Bashir, R., 2011.

Electrical detection of dsDNA and polymerase chain reaction amplification. Biomed. Microdevices 13, 973-982.

Schwan, H.P., 1996. Alternating current electrode polarization. Biophysik 3, 181-201.

Pournajaf, A., Ardebili, A., Goudarzi, L., Khodabandeh, M., Narimani, T., Abbaszadeh, H., 2014. PCR-based identification of methicillin-resistant *Staphylococcus aureus* strains and their antibiotic resistance profiles. Asian Pac J Trop Biomed 4(Suppl 1), S293-S297.

Ghanwate, N., Thakare, P., Bhise, P.R., Gawande, S., 2016. Colorimetric method for rapid detection of Oxacillin resistance in *Staphylococcus aureus* and its comparison with PCR for *mec A* gene. Sci. Rep. 6, 23013 (doi:10.1038/srep23013).

Stürenburg, E., 2009. Rapid detection of methicillin-resistant *Staphylococcus aureus* directly from clinical samples: methods, effectiveness and cost considerations. German Medical Science 7, Doc06 (ISSN 1612-3174).

Robicsek, A., Beaumont, J.L., Paule, S.M., Hacek, D.M., Thomson Jr., R.B., Kaul, K.L., King P., Peterson, L.R., 2008. Universal Surveillance for Methicillin-Resistant *Staphylococcus aureus* in 3 Affiliated Hospitals. Ann. Intern. Med. 148, 409-418.

Struelens, M.J., Hawkey, P.M., French, G.L., Witte, W., Tacconelli, E., 2009. Laboratory tools and strategies for methicillin-resistant *Staphylococcus aureus* screening, surveillance and typing: state of the art and unmet needs. Clin. Microbiol. Infect. 15, 112-119.

Hulme, J., 2017. Recent advances in the detection of methicillin resistant *Staphylococcus aureus* (MRSA). BioChip J. 11, 89-100.

McAdams, E.T., Lackermeier, A., McLaughlin, J., Macken, D., Jossinet, J., 1995. The linear

and non-linear electrical properties of the electrode-electrolyte interface. Biosens. Bioelectrons. 10, 67-74.

Gerwen, P.V., Laureyn, W., Laureys, W., Huyberechts, G., Beeck, M.O.D., Baert, K., Suls, J., Sansen, W., Jacobs, P., Hermans, L., Mertens, R., 1998. Nanoscaled interdigitated electrode arrays for biochemical sensors. Sens. Actuators, B 49, 73-80.

McClure, J., Zhang, K., 2017. Complete Genome Sequence of the Methicillin-Resistant *Staphylococcus aureus* Colonizing Strain M92. Genome Announc. 5, e00478-17.

Fig. 1. Impedance change corresponding to NaCl (sodium chloride) concentration. The impedance was measured using nanogap electrodes with 70, 150, 300, 500 nm and microcap electrode with 2 um gap, respectively.

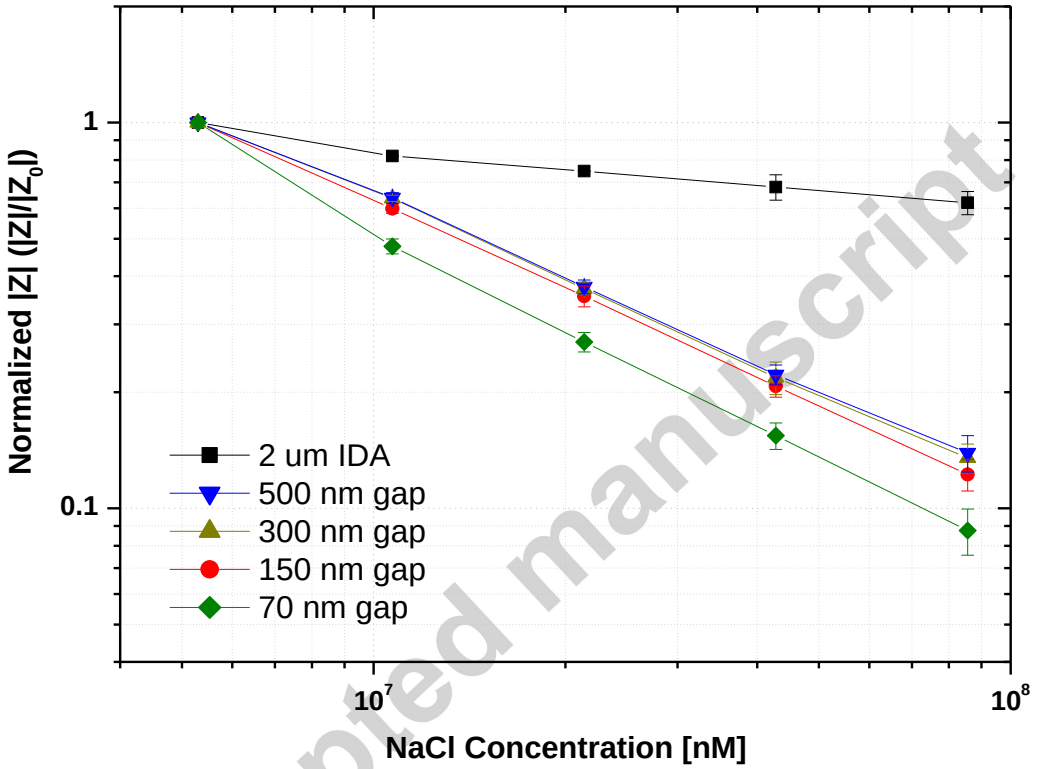

Fig. 2. Bode plot of bulk solution impedance with frequency response according to DNA (Deoxyribonucleic acid) amplification. (a) 70 nm nanogap and (b) 2 μm microgap sensor for 5 μl of the 260 pM *mecA* gene (template DNA).

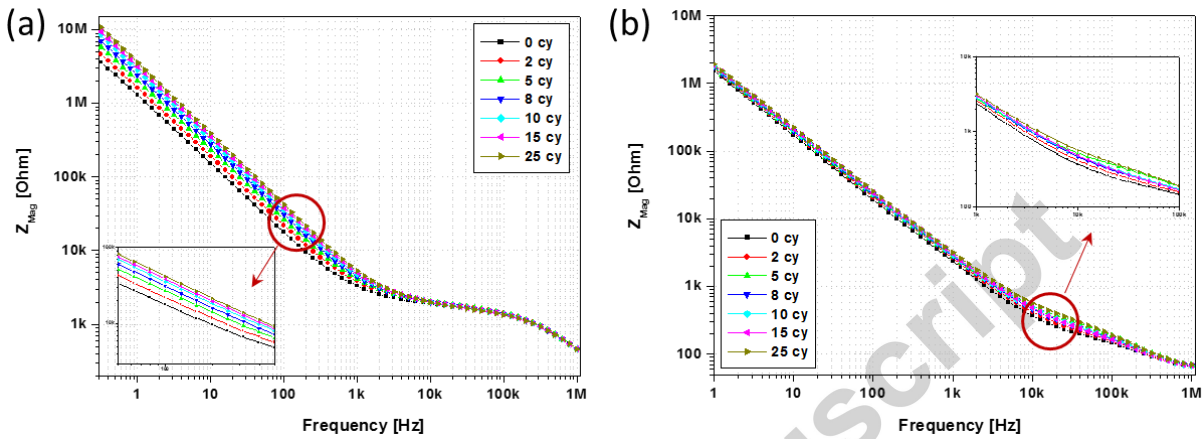

Fig. 3. Sensitivity of the nanogap electrode vs. the microgap electrode (Black: 2 μm IDA (interdigitated array) microgap electrode, Red: 70 nm nanogap electrode, closed triangle: 260 pM *mecA* gene template, closed circle: no template). (PCR is polymerase chain reaction).

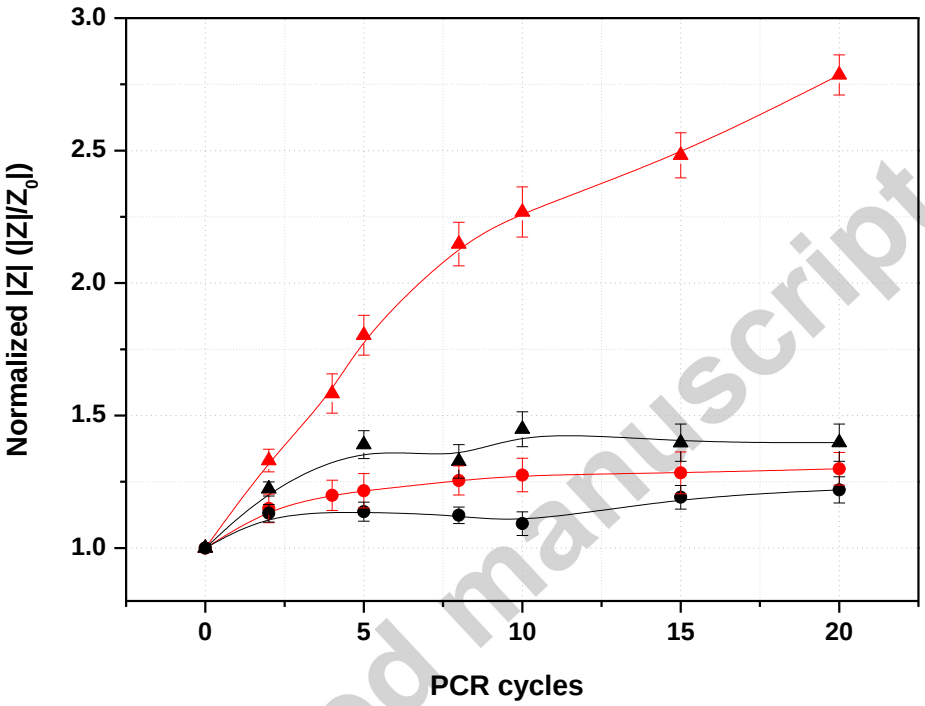

Fig. 4. Normalized impedance changes upon DNA amplification during PCR (polymerase chain reaction) cycle with the same 70 nm gap sensor. The initial concentrations of the *mecA* gene template in each sample were from 0 (no template) to 260 pM.

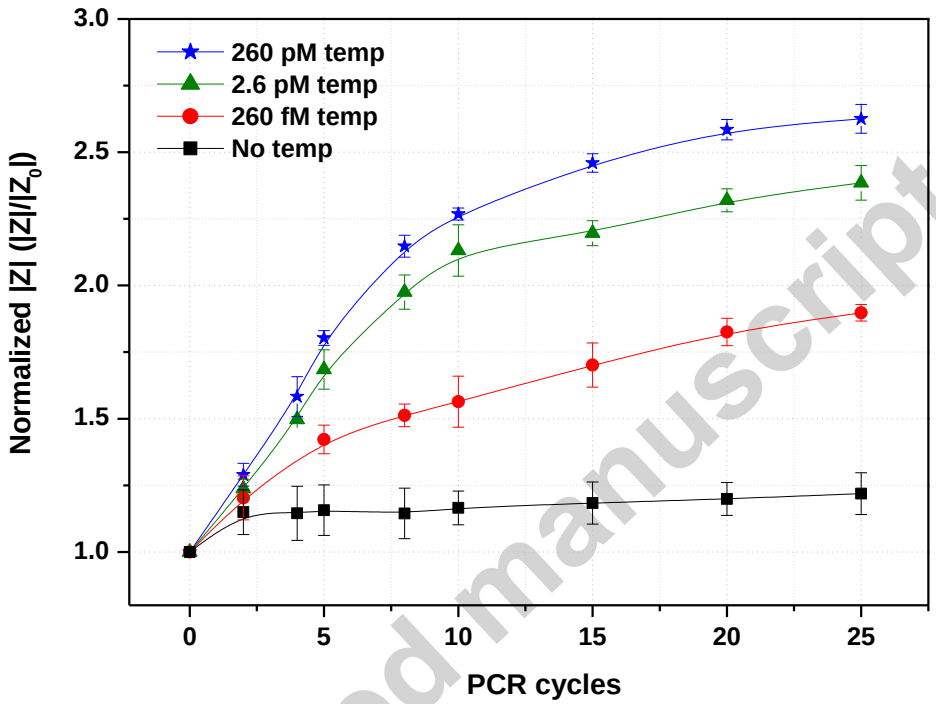

Fig. 5. Effect of the gap size on the performance of the nanogap-based impedimetric sensor. (PCR solution included 260 pM template originally.)

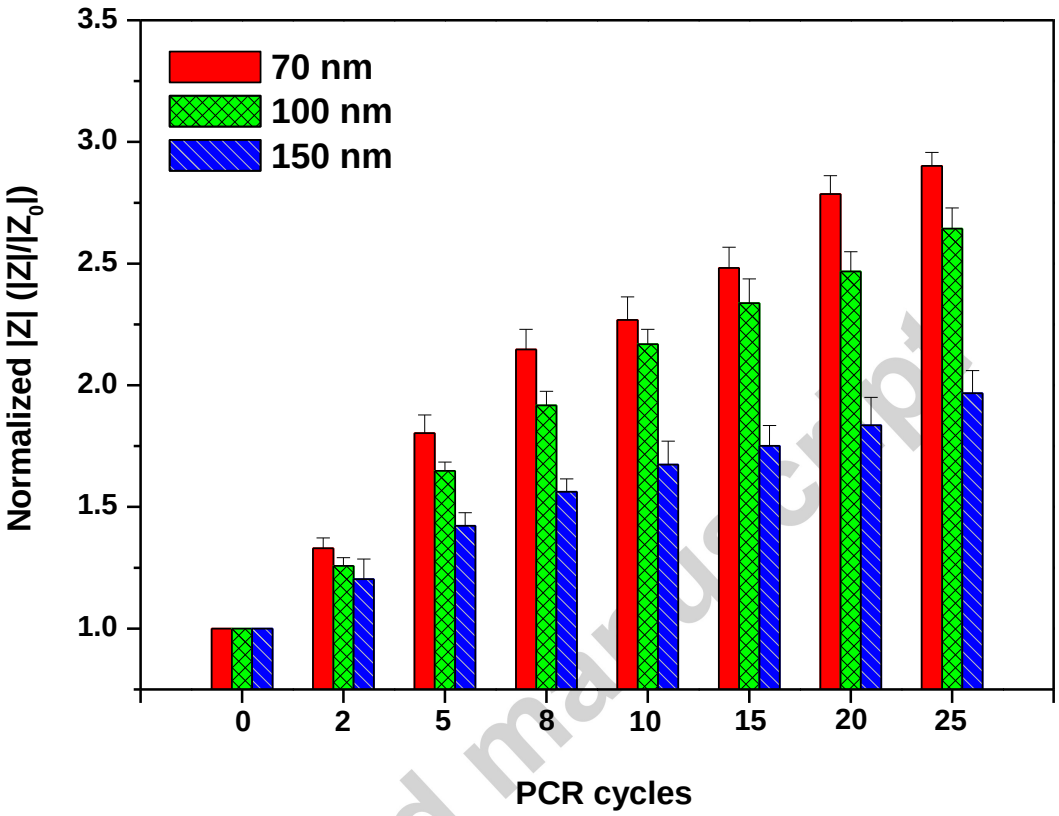

Fig. 6. (a) Relative intensity of the PCR product with 531 fM genomic DNA (gDNA) from methicillin-resistant *Staphylococcus aureus* (MRSA) originally. (b) Direct assay of impedance change according to mecA gene amplification with the same sample. The background red line was ascribed from the impedance value of 25th PCR product with gDNA from *Staphylococcus aureus* (SA).

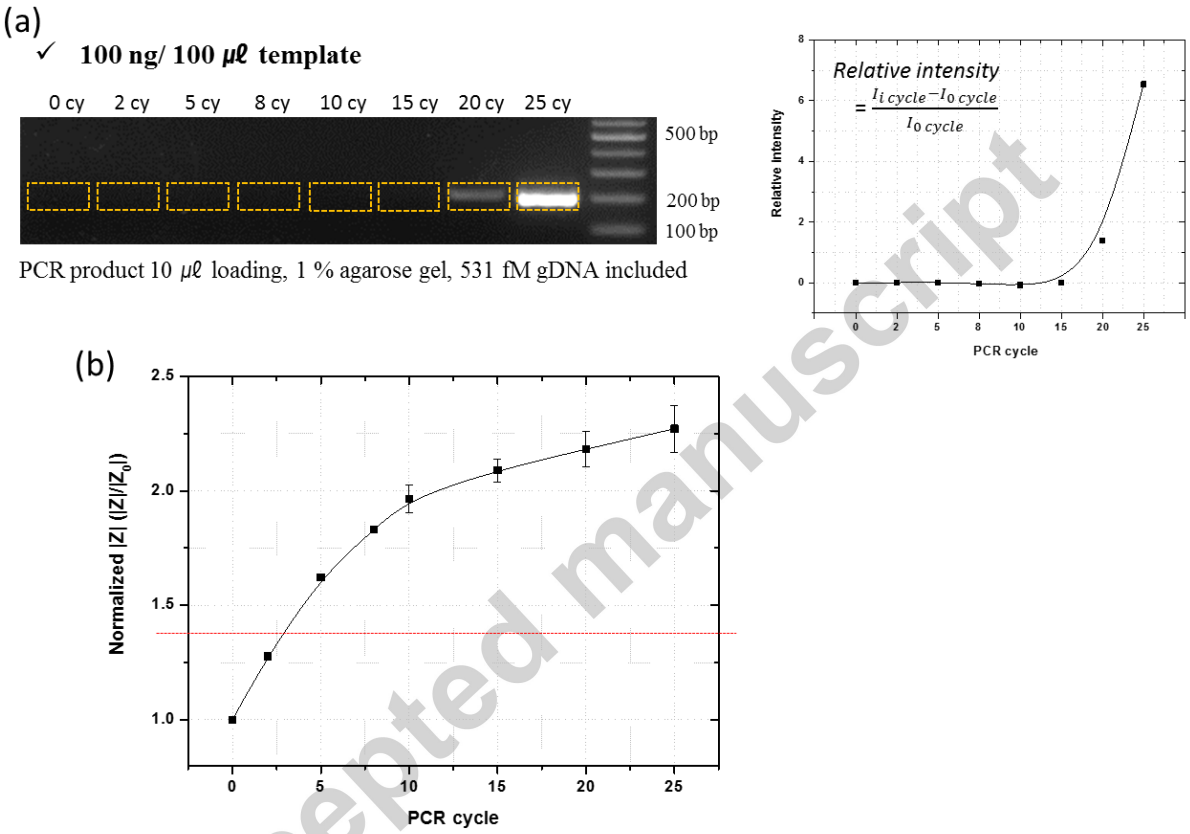

Highlights:

- Direct analyze the bulk solution impedance of PCR products according to different amounts of the amplified *mecA* gene without any purification using nanogap-based sensor
- A much narrower (70 nm) nanogap electrode-based impedimetric sensor could detect the DNA amplification fast in 5th PCR cycle even in 260 fM of target DNA template originally
- 70 nm nanogap sensor achieved the maximum 7-fold superior sensitivity to microgap electrode sensor and detected the amplification of genomic DNA which was extracted from MRSA successfully
- The experimental data matched well to theoretical fitting